



Building Better Spin Models for Merging Binary Black Holes: Evidence for Nonspinning and Rapidly Spinning Nearly Aligned Subpopulations

Shanika Galaudage^{1,2} , Colm Talbot³ , Tushar Nagar^{1,2} , Deepnika Jain⁴, Eric Thrane^{1,2} , and Ilya Mandel^{1,2,5} ¹ School of Physics and Astronomy, Monash University, Clayton VIC 3800, Australia; shanika.galaudage@monash.edu² OzGrav: The ARC Centre of Excellence for Gravitational Wave Discovery, Clayton VIC 3800, Australia³ LIGO Laboratory, California Institute of Technology, Pasadena, CA 91125, USA⁴ National Institute of Technology Karnataka, Surathkal, Srinivasnagar, 57025, India⁵ Institute of Gravitational Wave Astronomy and School of Physics and Astronomy, University of Birmingham, Birmingham, B15 2TT, UK

Received 2021 September 6; revised 2021 October 7; accepted 2021 October 11; published 2021 October 29

Abstract

Recent work paints a conflicting portrait of the distribution of black hole spins in merging binaries measured with gravitational waves. Some analyses find that a significant fraction of merging binaries contain at least one black hole with a spin tilt $>90^\circ$ with respect to the orbital angular momentum vector, which has been interpreted as a signature for dynamical assembly. Other analyses find that the data are consistent with a bimodal population in which some binaries contain black holes with negligible spin while the rest contain black holes with spin vectors preferentially aligned with the orbital angular momentum vector. In this work, we scrutinize models for the distribution of black hole spins to pinpoint possible failure modes in which the model yields a faulty conclusion. We reanalyze data from the second LIGO–Virgo gravitational-wave transient catalog (GWTC-2) using a revised spin model, which allows for a subpopulation of black holes with negligible spins. In agreement with recent results by Roulet et al., we show that the GWTC-2 detections are consistent with two distinct subpopulations. We estimate that 69%–90% (90% credible interval) of merging binaries contain black holes with negligible spin $\chi \approx 0$. The remaining binaries are part of a second subpopulation in which the spin vectors are preferentially (but not exactly) aligned to the orbital angular momentum. The black holes in this second subpopulation are characterized by spins of $\chi \sim 0.5$. We suggest that the inferred spin distribution is consistent with the hypothesis that all merging binaries form via the field formation scenario.

Unified Astronomy Thesaurus concepts: [Astrophysical black holes \(98\)](#); [Gravitational wave astronomy \(675\)](#)

1. Introduction

Gravitational waves from merging binaries encode information about the mass and spin of the component black holes and/or neutron stars. These properties, in turn, provide clues as to how the binary formed. Two scenarios are frequently invoked to explain merging binary black holes: field and dynamical (see Mandel & Farmer 2018; Mandel & Broekgaarden 2021; Mapelli 2021 for reviews). In the field scenario, binary black hole (BBH) systems are formed from isolated stellar binaries. In the dynamical scenario, BBH systems are assembled through interactions in dense stellar environments such as globular clusters and nuclear clusters; see Mapelli (2020) for a recent review.

These two scenarios yield distinct predictions for the distribution of black hole spin vectors. Field binaries are generally expected to form BBH systems with dimensionless spin vectors χ_1, χ_2 preferentially aligned with the orbital angular momentum vector \mathbf{L} . Supernova kicks may serve to somewhat misalign the $\chi_{1,2}$ and \mathbf{L} vectors, but the typical misalignment angle is expected to be modest (Rodriguez et al. 2016; O’Shaughnessy et al. 2017; Stevenson et al. 2017; Gerosa et al. 2018; Bavera et al. 2020). Dynamically assembled binaries, on the other hand, are expected to form BBH systems with isotropically distributed spin vectors (Kalogera 2000; Mandel & O’Shaughnessy 2010; Rodriguez et al. 2016, 2018; Talbot & Thrane 2017; Zevin et al. 2017; Doctor et al. 2019). These two

predictions can be used to estimate the fraction of merging binaries associated with each channel.

Using data from the second LIGO–Virgo gravitational-wave transient catalog (GWTC-2) (Abbott et al. 2021a), Abbott et al. (2021b) fit the distribution of χ_1, χ_2 with two different models, which produced qualitatively similar results. The DEFAULT model incorporates the spin magnitude model from Wysocki et al. (2019):

$$\pi(\chi_{1,2}|\alpha_\chi, \beta_\chi) = \text{Beta}(\chi_{1,2}|\alpha_\chi, \beta_\chi). \quad (1)$$

Here, $\chi_{1,2} \equiv |\chi_{1,2}|$ are the magnitudes of the dimensionless spin vectors, $\pi(\dots)$ denotes a prior probability density function, and α_χ, β_χ are hyperparameters⁶ controlling the shape of the Beta distribution, which is defined on the interval $\chi \in [0, 1]$ and constrained to only allow nonsingular distributions ($\alpha_\chi, \beta_\chi \geq 1$). The spin tilt distribution, meanwhile, is from Talbot & Thrane (2017):

$$\pi(z_{1,2}|\zeta, \sigma_r) = \zeta G_r(z_{1,2}|\sigma_r) + (1 - \zeta) \mathcal{J}(z_{1,2}), \quad (2)$$

where $z_{1,2} \equiv \cos \theta_{1,2}$ and $\theta_{1,2}$ are the misalignment angles between the orbital angular momentum vector and the respective spin vectors. Here G_r is a Gaussian distribution with a peak at $z = 1$ (aligned) and a width of σ_r , truncated at $z = [-1, 1]$. This submodel represents a population of preferentially aligned field binaries. Meanwhile, \mathcal{J} is a uniform distribution on the interval $z \in [-1, 1]$. This submodel represents an isotropic distribution

Original content from this work may be used under the terms of the [Creative Commons Attribution 4.0 licence](#). Any further distribution of this work must maintain attribution to the author(s) and the title of the work, journal citation and DOI.

⁶ For convenience, we later reparameterize the Beta distribution in terms of the spin magnitude mean μ_χ and standard deviation σ_χ .

associated with dynamical formation. The hyperparameter ζ is a mixing fraction determining the relative importance of each submodel.⁷ The final two spin degrees of freedom ϕ_1 , ϕ_2 describing the azimuthal directions of the spin vectors are assumed to be uniformly distributed.

In this paper we do not carry out calculations using the second model from Abbott et al. (2021b)—the GAUSSIAN model (Roulet & Zaldarriaga 2019; Miller et al. 2020). However, we argue below that it shares key features with the DEFAULT model. We therefore expect that our findings obtained with the DEFAULT model are applicable to results obtained with the GAUSSIAN model as well.

Using the DEFAULT model, Abbott et al. (2021b) reconstruct the distribution for the effective inspiral spin parameter

$$\chi_{\text{eff}} \equiv \frac{\chi_1 \cos \theta_1 + q \chi_2 \cos \theta_2}{1 + q}, \quad (3)$$

where $q \equiv m_2/m_1 \leq 1$ is the mass ratio, the distribution of which is modeled according to a power law:

$$\pi(q|\beta_q) \propto q^{\beta_q}. \quad (4)$$

The χ_{eff} parameter is frequently used to interpret results because it is an approximate constant of motion in precessing binaries and it is a relatively well-measured quantity. Abbott et al. (2021b) find that 12%–44% of BBH systems possess $\chi_{\text{eff}} < 0$ (90% credible interval), indicating that at least one black hole tilt angle $> 90^\circ$.

However, this finding is disputed by Roulet et al. (2021). These authors analyze a slightly different set of events (chosen to be more confidently detected) using a distinct set of posterior samples. They carry out two analyses of black hole spin. We focus for the moment on their “model-free” analysis, which assumes that χ_{eff} is uniformly distributed on the interval $[-1, 1]$. The prior for the poorly measured variable

$$\chi_{\text{diff}} \equiv \frac{q\chi_1 \cos \theta_1 - \chi_2 \cos \theta_2}{1 + q}, \quad (5)$$

is chosen to be uniform, conditioned on χ_{eff} and subject to the constraint that $\chi_{1,2} \leq 1$ as required by general relativity.⁸ This leaves four degrees of freedom χ_{ix} , χ_{iy} (where $i = 1, 2$), which are assumed to be uniformly distributed on a disk with radius $\sqrt{1 - \chi_{iz}^2}$. We call this set of assumptions ROULET+.

Using these distributions, Roulet et al. (2021) plot the credible intervals for χ_{eff} for individual events in their catalog. We reproduce this “dot plot” in Figure 1 for the events in Abbott et al. (2021b), using posterior samples from that study.⁹ Individual event posteriors computed using priors from different population models are represented with different colors: black is the fiducial LIGO–Virgo spin prior (uniform in χ_1 , χ_2 with an isotropic prior for the spin directions), green is the population model from Roulet et al. (2021), and pink is the DEFAULT model from Abbott et al. (2021b; averaged over the posterior on the population parameters).

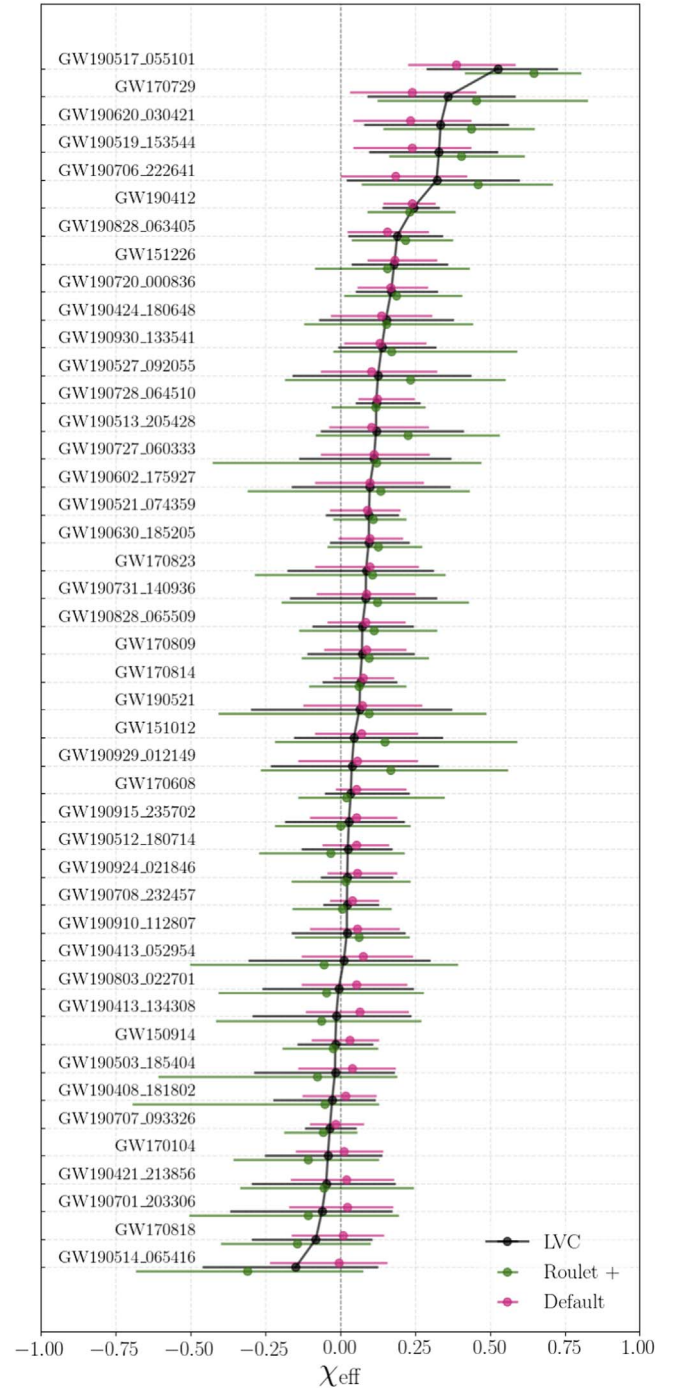


Figure 1. A “dot plot” showing the medians and 90% credible intervals for χ_{eff} assuming different population models. The fiducial model used by LIGO–Virgo (LVC, black) assumes uniform distribution for dimensionless spins χ_1 , χ_2 with an isotropic prior for the spin directions. Green (ROULET+) shows the model from Roulet et al. (2021). The DEFAULT model from Abbott et al. (2021b) is shown in pink. No models indicate support for a subpopulation of events with $\chi_{\text{eff}} < 0$.

By inspecting a version of this plot, Roulet et al. (2021) find there is not clear support for a population of events with $\chi_{\text{eff}} < 0$. Under all three population models, there are no events that have exclusively negative χ_{eff} support inconsistent with zero. We therefore concur with Roulet et al. (2021) that the BBH mergers observed to date are consistent with a subpopulation of negligible-spin events $\chi_{1,2} \approx 0$ with a second subpopulation of events with $\chi_{\text{eff}} > 0$. The signature from Abbott et al. (2021b) for a

⁷ Other possible formation channels (e.g., hierarchical triple systems, formation in active galactic nuclei, and primordial black holes) have distinct spin predictions. However, this model focuses on the isolated binary and dynamical formation channels.

⁸ Given these constraints, the marginalized prior on χ_{diff} is not actually uniform.

⁹ Posterior samples from <https://dcc.ligo.org/LIGO-P2000223/public>.

subpopulation of $\chi_{\text{eff}} < 0$ seen by Abbott et al. (2021b) is likely due to a misspecification of the assumed population spin model. This paper therefore seeks to improve on the DEFAULT model by developing a more sophisticated model for black hole spin in order to better describe the data and to provide more reliable inferences.

The remainder of this paper is structured as follows. In Section 2, we discuss why checks in Abbott et al. (2021b), designed to validate the observation of a subpopulation with $\chi_{\text{eff}} < 0$, did not reveal the model-dependency of this result. In Section 3, we propose an improved black hole spin model (called EXTENDED) designed to address the shortcomings of the DEFAULT model. We repeat the black hole spin distribution analysis from Abbott et al. (2021b; Section 4) using the EXTENDED model and report results in Section 5. In agreement with Roulet et al. (2021), we show that the observation of a subpopulation with $\chi_{\text{eff}} < 0$ is model-dependent. We present revised fits to the distribution of black hole spins. We conclude in Section 6 by discussing strategies for future development and testing of black hole spin models.

2. Diagnosing Limitations of the DEFAULT Model

Abbott et al. (2021b) include several checks, which would seem at first glance to support the claim for a subpopulation of events with $\chi_{\text{eff}} < 0$. First, they note the similar reconstructed distributions for χ_{eff} obtained with two different models: the DEFAULT model described above and GAUSSIAN model that describes the distribution of χ_{eff} and the effective precession spin parameter χ_p using a multivariate Gaussian (see their Figure 11(b)). The potential for model-induced systematic error is reduced given that the signature is visible using two different models. Second, they carry out posterior predictive checks to show that mock source populations drawn from the GAUSSIAN model would have similar distributions of χ_{eff} and χ_p to the observed data; see their Figure 26. Third, they perform an analysis in which a new hyperparameter $\chi_{\text{eff}}^{\text{min}}$ is added to the population model, which enforces a minimum value of $\chi_{\text{eff}} > \chi_{\text{eff}}^{\text{min}}$; see their Figure 27. A negative value for $\chi_{\text{eff}}^{\text{min}}$ is preferred over $\chi_{\text{eff}}^{\text{min}} = 0$, seemingly bolstering the case for a subpopulation of events with $\chi_{\text{eff}} < 0$.

It is instructive to discuss how each of these checks fails to catch the apparent lack of $\chi_{\text{eff}} < 0$ events in Figure 1. While the agreement between the DEFAULT and GAUSSIAN models provides something of a sanity check, both models lack a key feature: the ability to account for an excess of BBH systems with $\chi_{1,2} \approx 0$. The possibility that some fraction of LIGO–Virgo binaries should merge with negligible spin is supported by theoretical studies of angular momentum transport (Fuller & Ma 2019; Belczynski et al. 2020). Moreover, the negligible spin of many/most LIGO–Virgo binaries has been noted observationally (Miller et al. 2020; Kimball et al. 2021). Neither spin model from Abbott et al. (2021b) accounts for a subpopulation of binaries with $\chi \approx 0$ black holes. Since neither model can accommodate an excess of events with $\chi_{1,2} \approx 0$, the models are liable to fit such an excess with the next best thing: a subpopulation of events distributed *about* $\chi_{\text{eff}} = 0$. In this way, the DEFAULT and GAUSSIAN models can both yield false positive signals for $\chi_{\text{eff}} < 0$ when the true population contains an excess of events with $\chi_{1,2} \approx 0$.

Next we turn to the posterior predictive check from Abbott et al. (2021b), their Figure 26. This plot compares the cumulative distribution of χ_{eff} for the data to the distribution expected from the model. The two distributions are visually

consistent. While a mismatch between data and model predictions would indicate a failure of the model, a match does not prove that the model is a faithful representation of the data. Using a different population model, Roulet et al. (2021) find no evidence for a subpopulation of events with $\chi_{\text{eff}} < 0$ —a finding that we confirm independently below.

Finally, we consider the test from Abbott et al. (2021b) showing that the data prefer negative values of $\chi_{\text{eff}}^{\text{min}}$ such that some events in the population are characterized by negative χ_{eff} values on the interval $(\chi_{\text{eff}}^{\text{min}}, 0)$ (see their Figure 27). It should now be apparent that this test can be tricked if the data contain an excess of events with $\chi_{1,2} \approx 0$. In order to illustrate this—and to build an improved model for BBH spin—we introduce an EXTENDED model, which incorporates elements from Roulet et al. (2021) that enable an excess of negligible-spin events.

3. The EXTENDED Model

We introduce two changes to the DEFAULT model. First, we add a new population parameter λ_0 , corresponding to the fraction of BBH mergers with negligible spin. Our revised spin magnitude distribution is

$$\pi(\chi_{1,2} | \alpha_\chi, \beta_\chi, \lambda_0) = (1 - \lambda_0) \text{Beta}(\chi_{1,2} | \alpha_\chi, \beta_\chi) + \lambda_0 G_t(\chi_{1,2} | \mu = 0, \sigma_0), \quad (6)$$

where G_t is a truncated Gaussian distribution peaking at $\chi_{1,2} = 0$ with width σ_0 . We set $\sigma_0 = 0$ so that the spin magnitudes are precisely zero and carry out the analysis using a dedicated set of zero-spin posterior samples. Setting $\chi = 0$ is probably a good approximation since Fuller & Ma (2019) suggest that typical black hole spin magnitudes are $\chi \approx 0.01$ (ignoring binary effects, particularly tidally induced spin-up, discussed by, e.g., Kushnir et al. 2016; Qin et al. 2018; Zaldarriaga et al. 2018; Bavera et al. 2020; Belczynski et al. 2020; Mandel & Fragos 2020). It would be interesting to make σ_0 a population parameter that can be fit with the data. However, we leave this for future work as there are some technical challenges; preliminary studies with small, nonzero values of σ_0 seem to suffer from undersampling effects. We adopt a uniform prior for λ_0 on the interval $[0, 1]$.

Our second change is to add a population parameter z_{min} to the distribution of black hole tilt angles such that the combined distribution from Equation (2) is forced to zero for $z_{1,2} < z_{\text{min}}$:

$$\pi(z_{1,2} | \zeta, \sigma_t, z_{\text{min}}) \propto (\zeta G_t(z_{1,2} | \sigma_t) + (1 - \zeta) \mathcal{J}(z_{1,2})) \Theta(z_{1,2} - z_{\text{min}}). \quad (7)$$

We adopt a uniform prior for z_{min} on the interval $[-1, 1]$. In Section 5 we present results of an analysis of events from the GWTC-2 catalog using the EXTENDED model. The full list of population hyperparameters and priors is given in Table 1.

4. Analysis

We use `GWPopulation` (Talbot et al. 2019) to obtain posterior distributions for the population parameters in the EXTENDED model using the same event list used in Abbott et al. (2021b). This data set consists of 44 confidently detected BBH mergers. It does not include GW190814 (Abbott et al. 2020a), which may be a neutron-star black hole binary and is a clear outlier from the rest of the population. The analysis from Abbott et al. (2021b) employed higher-order modes waveforms,

Table 1
Summary of EXTENDED Model Hyperparameters

Parameter	Description	Prior
λ_0	Mixing fraction of mergers with negligible spin, $\chi_{1,2} \lesssim \sigma_0$	$U(0, 1)$
σ_0	Spread in $\chi_{1,2}$ for systems with negligible spin	$\sigma_0 = 0$
μ_χ	Mean of spin magnitude distribution	$U(0, 1)$
σ_χ^2	The square of the width of the spin magnitude distribution	$U(0, 0.25)$
ζ	Mixing fraction of mergers with preferentially aligned spin	$U(0, 1)$
σ_t	Spread in projected misalignment for preferentially aligned black holes	$U(0, 4)$
z_{\min}	Minimum value of the projected misalignment	$U(-1, 1)$

Note. The notation $U(a, b)$ indicates a uniform distribution on the interval ranging from a to b .

which we are unable to use here for technical reasons. Instead, we use IMRPHENOMPV2 and IMRPHENOMD waveforms (Hannam et al. 2014; Husa et al. 2016; Khan et al. 2016) to obtain samples for $\chi > 0$ and $\chi = 0$ respectively. While this choice of waveforms is unlikely to affect our main conclusions, the different choice of waveform leads to subtle shifts in the posterior distribution of some population parameters. We estimate these shifts by comparing the DEFAULT model results with IMRPHENOMPV2 waveforms to the DEFAULT model results with higher-order mode waveforms. We determine that the typical values of χ for the subpopulation with spinning black holes would likely be lower by ~ 0.05 if we had used higher-order mode waveforms. Additional details are available in the companion repository.¹⁰ The GWPopulation package employs Bilby (Ashton et al. 2019; Romero-Shaw et al. 2020) and dynesty (Speagle 2020). We fit the distribution of black hole masses using the POWER LAW + PEAK model from Abbott et al. (2021b) adapted from Talbot & Thrane (2018). We fit the merger redshift distribution using the POWER-LAW EVOLUTION model from Abbott et al. (2021b), adapted from Fishbach et al. (2018). We employ two sets of posterior samples: one using the standard LIGO–Virgo priors and one generated using a zero-spin prior; see Kimball et al. (2021).¹¹ The zero-spin samples are necessary to avoid artifacts due to undersampling. Additional technical details are provided in the Appendix.

We adopt the same treatment of selection effects as used in Abbott et al. (2021b), which accounts for mass-dependent Malmquist bias, but not selection effects due to spin. The authors of that work explain that they cannot reliably estimate spin-induced selection effects using the currently available injection set; see their Appendix F. It is slightly easier to detect BBH signals with $\chi_{\text{eff}} > 0$, so we expect that our fit may slightly overemphasize high positive values of χ_{eff} relative to the true distribution. Figure 1 of Ng et al. (2018) illustrates this shift in the inferred χ_{eff} distribution. This shift will impact the branching ratio between the two nonspinning and spinning subpopulations. We estimate that including selection effects would decrease the estimated subpopulation of spinning BBHs by $\lesssim 20\%$ of the currently estimated fraction $(1 - \lambda_0)$, i.e., $\lesssim 4\%$.

¹⁰ Supplementary material including analysis inputs, posterior samples, and additional plots are available here: https://github.com/shanikagalaulage/bbh_spin.

¹¹ Astute readers may notice that Kimball et al. (2021) reports that the fraction of BBH systems with negligible spin is consistent with zero $\lambda_0 \approx 0$. In that study, the BBH events with measurable spin are likely attributed to a subpopulation containing one or more rapidly spinning “second-generation” black holes (formed from previous mergers). Thus, they likely do not influence the fit for first-generation dimensionless spin parameters, α_χ, β_χ , which are found to be consistent with a population of low-spin black holes.

Thus, the systematic error from selection effects is less than the current statistical uncertainty.

5. Results

We plot population predictive distributions (PPDs)¹² comparing the DEFAULT and EXTENDED models in Figure 2. In the left panel, we show the reconstructed spin magnitude distribution, the EXTENDED model exhibits clear support for a narrow peak at $\chi_{1,2} = 0$, which is not present in the DEFAULT model because the model lacks the flexibility to fit this peak. In the right panel, we show the reconstructed distribution of the (cosine of the) spin tilts, we see that the EXTENDED model distribution of $z_{1,2} \equiv \cos \theta_{1,2}$ tapers off for $\cos \theta_{1,2} \lesssim 0$ while the DEFAULT model exhibits considerably more support for binaries with $\cos \theta_{1,2} < 0$. Since the EXTENDED model includes the DEFAULT model as a special case (with $\lambda_0 = 0, z_{\min} = -1$), we conclude that the data prefer a subpopulation of binaries with $\chi_{1,2} \approx 0$ over a subpopulation of binaries with $\chi_{\text{eff}} < 0$. This conclusion is supported by our model selection results, summarized in Table 2, which show the EXTENDED model is preferred over the DEFAULT model by $\log_{10} \mathcal{B} \approx 22.7$. This preference clearly comes from the introduction of a zero-spin subpopulation (see the $\lambda_0 = 0$ model). There is a slight preference for the EXTENDED model with a broad uniform prior on z_{\min} or with z_{\min} fixed to zero than with z_{\min} fixed to -1 .

Figure 3 shows the posterior distributions for the two variables new to the EXTENDED model: z_{\min} (left) and λ_0 (right). Turning first to the posterior for z_{\min} , we find ample posterior support for $z_{\min} = 0$, which means the data are consistent with the premise that all merging binaries have $\chi_{\text{eff}} > 0$. Next we turn our attention to the posterior distribution for λ_0 (right), the parameter that controls the fraction of binaries merging with negligible black hole spin. The distribution shows that most BBH systems merge with negligible spins: $\lambda_0 = 0.81_{-0.12}^{+0.09}$ (90% credibility).

In Figure 4 we include a corner plot showing the posterior distribution for all the population parameters in the EXTENDED model. The navy contours mark the $1\sigma, 2\sigma,$ and 3σ credible intervals for the EXTENDED model while the pink contours show the results for the DEFAULT model used in Abbott et al. (2021b). There are a number of interesting differences between the two models. First, the μ_χ parameter, which determines the average dimensionless spin magnitude for black holes (those with nonnegligible spin in the EXTENDED model), shifts from

¹² The PPD is given by the conditional prior marginalized over the posterior distribution of the population parameter

$$p_\Lambda(\chi_{1,2}|d) = \int d\Lambda p(\Lambda|d) \pi(\chi_{1,2}|\Lambda). \quad (8)$$

Here, Λ are population parameters described in Table 1.

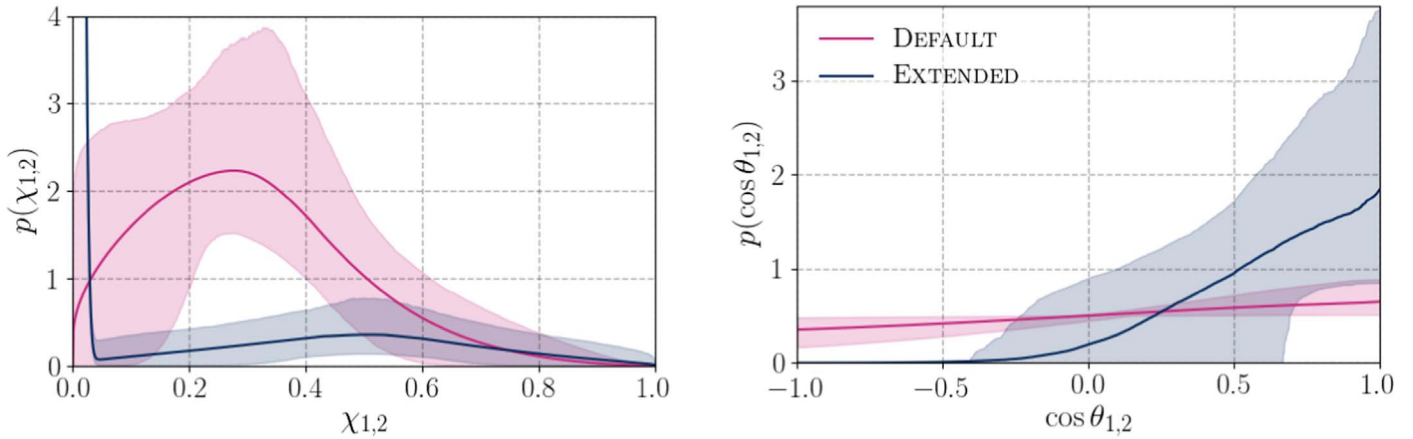


Figure 2. Population predictive distributions for the DEFAULT (pink) and the EXTENDED (navy) models. Left: the distribution of dimensionless spin. Right: the distribution of the cosine of the tilt angle. The solid curves represent the mean and the shaded region represents the 90% credible interval. In the left-hand panel, we represent the EXTENDED model’s delta function at $\chi = 0$ zoomed in, with a narrow Gaussian and a width of $\sigma_0 = 0.01$ for visibility.

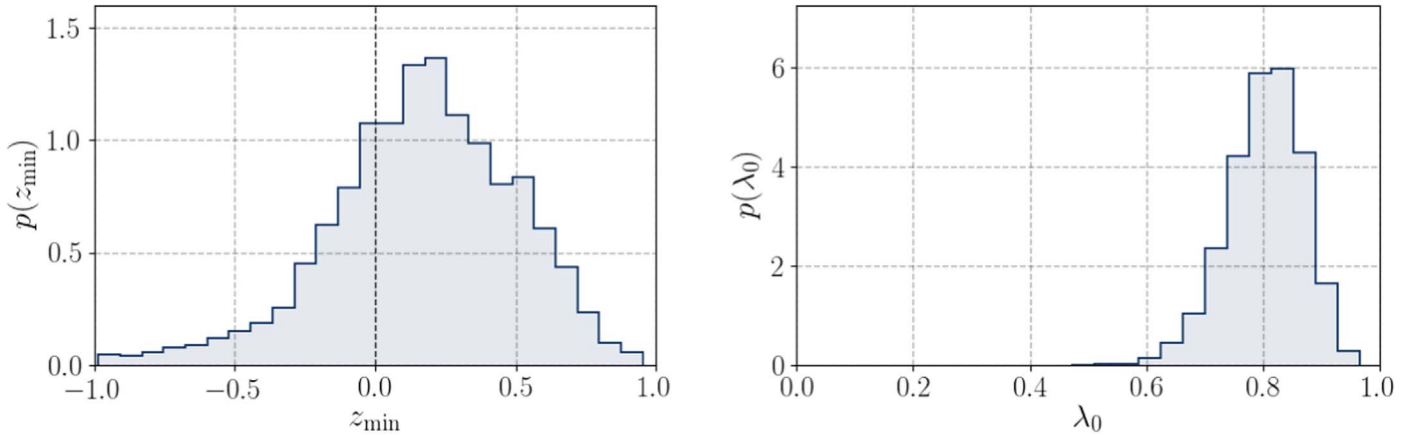


Figure 3. Posterior distributions for population parameters new to the EXTENDED model. Left: the posterior distributions for the population parameter z_{\min} , which determines the minimum cosine tilt angle such that $\cos \theta_{1,2} \geq z_{\min}$. Right: the posterior distribution for λ_0 , the fraction of binaries with negligible black hole spins $\chi_{1,2} = 0$.

Table 2

Log Bayes Factors and Maximum Log Likelihood Differences for Different Spin Models Compared to the DEFAULT Model

Spin Model	$\log_{10} \mathcal{B}$	$\Delta \log_{10} \mathcal{L}_{\max}$
DEFAULT	0.00	0.00
EXTENDED	22.67	22.34
EXTENDED with $z_{\min} = 0$	22.92	22.45
EXTENDED with $z_{\min} = -1$	21.80	22.24
EXTENDED with $\lambda_0 = 0$	0.63	0.55

≈ 0.3 for DEFAULT to ≈ 0.5 for EXTENDED. This shift reflects the fact that dimensionless spin is higher when we allow for a separate population of binaries with negligible black hole spin. Taken together, Figures 3 and 4 suggest two subpopulations: the majority of BBH systems merge with negligible spin while a minority merge with moderately large spins.

Second, the posterior for the ζ parameter (shown in Figure 4), which determines the fraction of binaries with preferentially aligned spin, becomes broader, approaching a uniform distribution. This change is explained by the introduction of the z_{\min} parameter, which provides a new means of building a population

of preferentially aligned binaries.¹³ Both models disfavor perfect alignment of the black hole spin vectors with the orbital angular momentum. The DEFAULT model shows support for a preferentially aligned population ($\zeta > 0$) but with nonzero misalignment angle spread ($\sigma_\tau > 0$). Meanwhile, the EXTENDED model favors a broad range of $z_{\min} = (-0.41, 0.67)$ at 90% credibility, so the misalignment distribution is likely not cut off at near-exact alignment.

Finally, in Figure 5, we show the χ_{eff} PPDs for the DEFAULT and EXTENDED models. The EXTENDED model is characterized by a sharp peak at $\chi_{\text{eff}} = 0$ corresponding to the subpopulation of BBH systems with negligible spin. While the EXTENDED PPD does not vanish for $\chi_{\text{eff}} < 0$, there is very limited support there, with fewer than 0.2% of all binaries predicted to have $\chi_{\text{eff}} < -0.1$. This is consistent with Figure 1, which shows no suggestion of events with negative χ_{eff} . This conclusion is also consistent with Figure 3, which shows support for z_{\min} as low as $z_{\min} \approx -0.5$. However, the same plot shows that the data are consistent with $z_{\min} = 0$. In other

¹³ Consider, for example, the case where $z_{\min} \approx 0$ and $\zeta = 0$, which is well-supported by the data. This case corresponds to a population where black hole tilts are “half-isotropically” distributed for angles $\theta_{1,2} < 90^\circ$, but black holes never merge with tilt angles $> 90^\circ$.

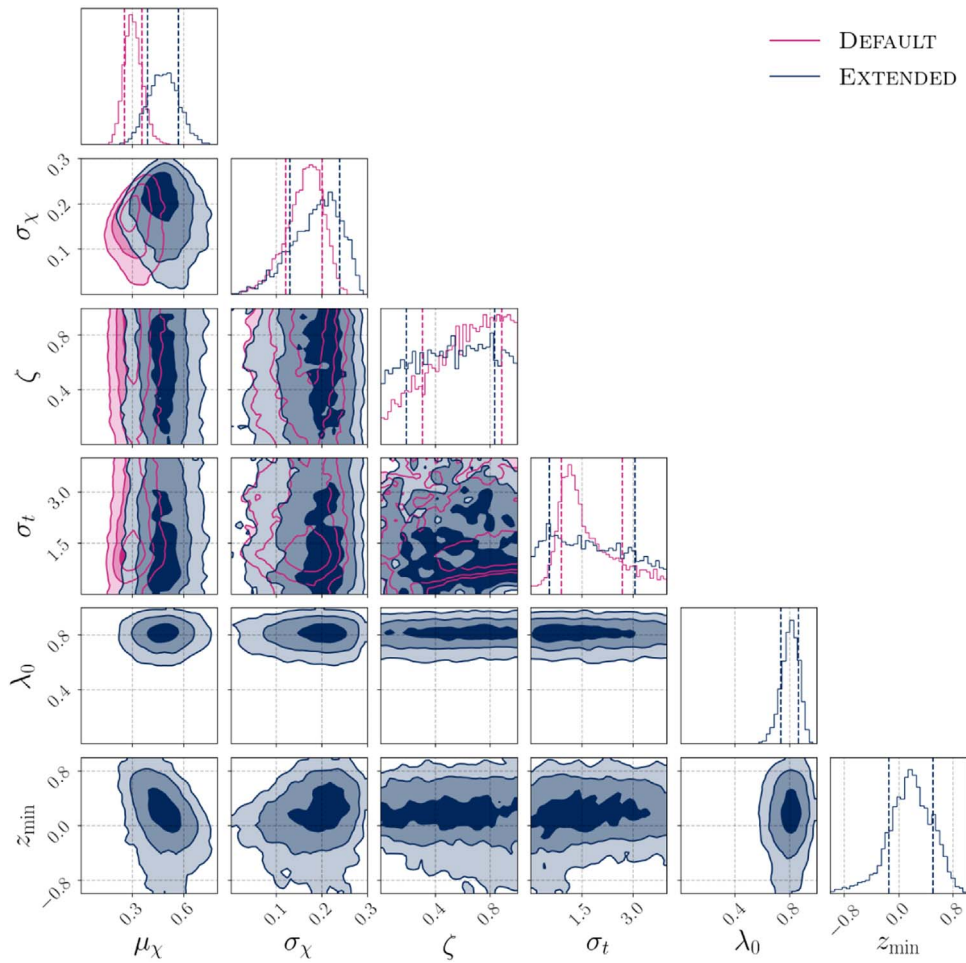


Figure 4. A corner plot showing hyperposterior distributions for the DEFAULT (pink) and EXTENDED (navy) models. The parameters are summarized in Table 1. The shaded regions represent 1σ , 2σ , and 3σ credible intervals.

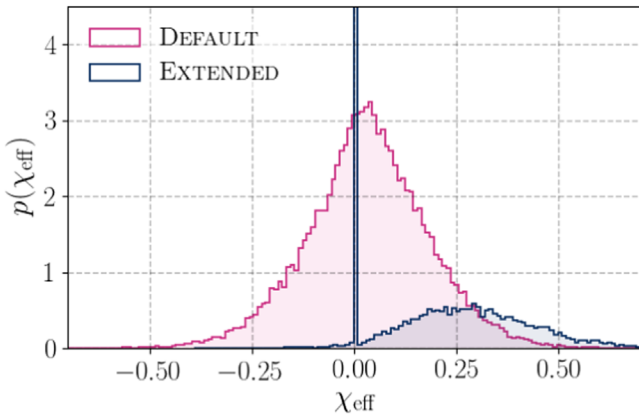


Figure 5. The population predictive distribution for the effective inspiral spin parameter χ_{eff} for the DEFAULT (pink) and the EXTENDED (navy) models.

words, we cannot rule out the possibility of a small subpopulation with $\chi_{\text{eff}} < 0$, but the EXTENDED model provides no evidence that such a subpopulation exists. We also performed a set of population predictive checks, which shows the model is a good fit to the data; these figures are available in the companion repository. However, we emphasize that a match of the predicted and observed distributions does not guarantee the model accurately represents the data.

6. Discussion

Inspired by Roulet et al. (2021), we reanalyze the population of merging binary black holes from Abbott et al. (2021b) using a revised model for the distribution of black hole spins designed to allow for a subpopulation with negligible spin. Using the same events and the same posterior samples as Abbott et al. (2021b), we obtain results qualitatively similar to Roulet et al. (2021), suggesting that Abbott et al.’s (2021b) finding of a subpopulation of binaries merging with $\chi_{\text{eff}} < 0$ is model-dependent. Using our new EXTENDED model, we find that the data can be explained by the hypothesis that all binaries merge with black hole spin preferentially aligned with the orbital angular momentum or with negligible spin. These findings are consistent with GWTC-1 studies (Farr et al. 2017, 2018; Abbott et al. 2019; García-Bellido et al. 2021) inferring the population of what was then 10 BBH detections is consistent with mostly negligible spins and a few events with support for $\chi_{\text{eff}} > 0$.

This result somewhat diminishes the case for dynamical mergers as a major channel for merging binaries. However, the dynamical scenario remains a plausible explanation for binary mergers with black holes in the pair instability mass gap (Abbott et al. 2020b). If GW190521 is a hierarchical merger (assembled from the products of previous mergers), perhaps black holes participating in the first generation of dynamical mergers are among the $\approx 80\%$ with negligible spin. Indeed, studies of

dynamical mergers in dense clusters find that small spins are required for first-generation black holes in order for their remnants to be retained to merge again (Kimball et al. 2020, 2021). If a large fraction of merging binaries is assembled dynamically, our results suggest that most dynamically merging black holes have negligible spin.

A subpopulation of binaries with negligible black hole spins can also be accommodated within the field formation framework; see, e.g., Belczynski et al. (2020) and Bavera et al. (2020). If the stellar progenitors of BBH systems efficiently shed angular momentum through mass loss, it may be common for most field BBH systems to form with negligible spin. A minority of progenitors in sufficiently tight binaries could, however, tidally spin up the stellar core of the secondary star prior to its collapse into a black hole, producing a BBH system with at least one rapidly spinning BH. In this framework, black holes with nonnegligible spins could be those whose naked helium star progenitors were tidally spun up in tight binaries. This possibility can be explored in the future by relaxing the assumption that the spins and spin-orbit misalignment angles of both binary components are independently drawn from the same distributions.

Binary black hole detections in which the more massive black hole clearly has nonzero spin $\chi_1 > 0$ could be challenging to accommodate in the standard field framework as described above (Mandel & Fragos 2020; Qin et al. 2021). Several events in GWTC-2 would seem to fall into this category, including GW151226 (Abbott et al. 2016; Chia et al. 2021, but see Mateu-Lucena et al. 2021), GW190412 (Abbott et al. 2020c; Zevin et al. 2020, but see Mandel & Fragos 2020), and GW190403_051519 (Abbott et al. 2021c; Qin et al. 2021, though the high mass already makes field formation unlikely for this system). If these systems formed in the field, it is possible that the more massive black hole formed from what was initially the secondary (lower mass) star that subsequently gained mass through accretion. In this scenario, the secondary star could still be tidally spun up before collapsing into the more massive black hole, a scenario explored in Bavera et al. (2021) and Olejak & Belczynski (2021). Furthermore, the progenitor of the first-formed black hole can also be tidally spun up if the binary is initially very compact, as appears to be the case with high-mass X-ray binaries such as M33 X-7 (Valsecchi et al. 2010) and Cygnus X-1 (Qin et al. 2019); though it is unclear if such systems lead to merging BBHs (Neijssel et al. 2021).

In this work we focused only on the black hole spin distribution, assuming that the black hole mass distribution is independent. However, there may be possible correlations between mass and spin, as explored by Safarzadeh et al. (2020), Tagawa et al. (2021), and Callister et al. (2021). Examples include predictions for negative correlation between mass and spin for isolated binary evolution (e.g., Bavera et al. 2020) and mergers in young clusters (e.g., Kumamoto et al. 2021). Meanwhile, positive correlations are predicted for repeated dynamical mergers in globular clusters (e.g., Rodriguez et al. 2018) with a possible high-mass spin-aligned contribution from chemically homogeneously evolving binaries (e.g., Mandel & de Mink 2016; Marchant et al. 2016; Riley et al. 2021), while mergers in AGN disks may exhibit a positive correlation between mass and the dispersion of effective spin (Tagawa et al. 2020). Investigating such correlations, along with possible correlations with redshift, can improve the accuracy

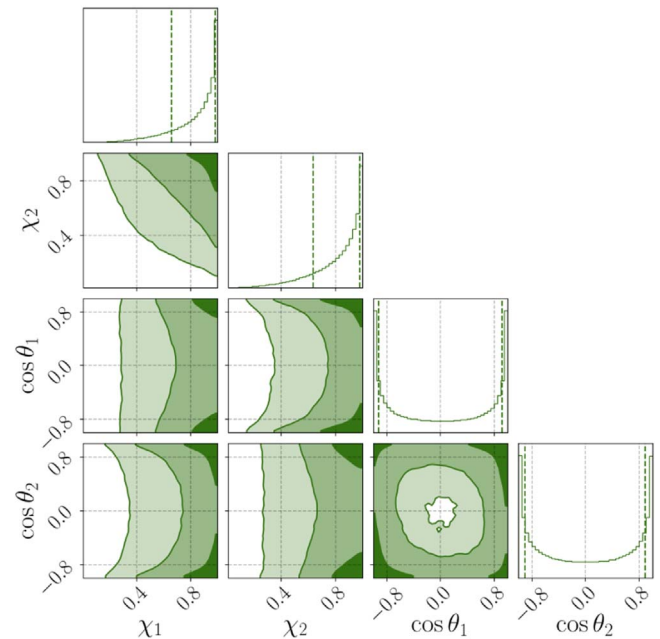


Figure 6. Prior distribution on spin magnitudes and cosine of the tilt angle for the Roulet et al. (2021) χ_{eff} model.

of the models and enable them to better distinguish between various evolutionary scenarios.

Our work highlights the subtleties in diagnosing model misspecification, which can lead to overly model-dependent conclusions. While Abbott et al. (2021b) perform a number of checks to validate their evidence for a subpopulation of events with $\chi_{\text{eff}} < 0$ (see Section 2), none of these checks pinpointed how the model could misbehave when applied to a distribution with a subpopulation of binaries with negligible-spin black holes, as pointed out by Roulet et al. (2021). We recommend careful consideration of possible sharp features—in this case, a narrow peak with $\chi_{1,2} \approx 0$ —since they can yield misleading results when fit with slowly varying functions.

The “dot plot” featured in Figure 1 of Roulet et al. (2021), and included in our own Figure 1, provides an important visual check. However, it is not obvious that such a plot can be applied more broadly to help spot model misspecification. For one thing, the χ_{eff} dot plot is fairly straightforward to interpret because the likelihood function for individual events is approximately Gaussian in this parameter. However, this is not true for other variables, for example, χ_p . Moreover, even the χ_{eff} dot plot includes a hidden population model, which can affect its interpretation.

In order to obtain a prior distribution that is uniform in χ_{eff} , the “model-free” prescription in Roulet et al. (2021) makes implicit assumptions about the distribution of the physical spin parameters χ_1 , χ_2 , $\cos \theta_1$, and $\cos \theta_2$. Plotting the distribution of these spin parameters in Figure 6, we see that some of the assumed distributions are not especially physical. In particular, the “model-free” analysis implicitly assumes that black holes preferentially spin near the Kerr limit $\chi_{1,2} = 1$ with a strong covariance between χ_1 and χ_2 . The distribution of spin tilts, meanwhile, favors spin vectors that are either aligned or antialigned with the orbital angular momentum vector. Comparing the green “Roulet +” model to the black LVC model in Figure 1, we see that the two models produce similar

dot plots when one accounts for the implicit preference for larger spins in the “model-free” approach. However, the two models do not produce the same ordered list when we rank events from smallest to largest χ_{eff} , which indicates that other spin degrees of freedom described by the implicit model influence this plot—an effect that will become more significant as the gravitational-wave catalog grows. However, the surprising shape of the distributions in Figure 6 reminds us that all fully specified models of black hole spin require some distribution of physical parameters even if these distributions are not explicit. It therefore seems useful to cast population models in terms of physical parameters, or, at the very least, to check the suitability of the distribution of physical parameters.

There are a number of interesting extensions to this work worthy of future exploration. Our EXTENDED model is designed to investigate questions raised in Abbott et al. (2021b) and Roulet et al. (2021). A number of possible model extensions consider more astrophysically motivated distributions. As discussed above, spin magnitudes and directions may be coupled with each other, or with mass and mass ratio (see, e.g., Callister et al. 2021). For example, there could be different spin magnitude distributions in the field scenario (preferentially aligned spins) and the dynamical scenario (isotropic spins). The low-spin-magnitude subpopulation could incorporate small but nonzero spins by varying σ_0 . The z_{min} parameter could be applied only to the subpopulation of binaries with $\cos\theta_{1,2}$ described by the truncated Gaussian distribution; this would restore the mixture model choice between a preferentially aligned distribution and an isotropic distribution.

We thank Tom Callister for his helpful comments during the preparation of this manuscript. Several authors are supported by the Australian Research Council (ARC) Centre of Excellence for Gravitational-wave Discovery (OzGrav), project number CE170100004. I.M. is the recipient of the ARC Future Fellowship FT190100574. The authors are grateful for computational resources provided by the LIGO Laboratory and supported by National Science Foundation Grants PHY-0757058 and PHY-0823459. This is document LIGO-P2100318.

Software: GWPopulation Talbot et al. (2019), Bilby Ashton et al. (2019); Romero-Shaw et al. (2020), dynesty Speagle (2020).

Appendix Implementing the EXTENDED Model with Zero-spin Samples

In this appendix we describe our implementation of inference on the EXTENDED model hyperparameters using two sets of posterior samples—one allowing for black hole spins (called “fiducial” samples), the other assuming zero black hole spins. Our starting point is the likelihood for the data d associated with a single gravitational-wave event given the population hyperparameters Λ :

$$\mathcal{L}(d|\Lambda) = \int d\chi_{1,2} \int dz_{1,2} \int d\eta \mathcal{L}(d|\chi_{1,2}, z_{1,2}, \eta) \times \pi(\chi_{1,2}|\alpha_\chi, \beta_\chi, \lambda_0) \pi(z_{1,2}|\zeta, \sigma_t, z_{\text{min}}) \pi(\eta|\Lambda). \quad (\text{A1})$$

Here, $\mathcal{L}(d|\chi_{1,2}, z_{1,2}, \eta)$ is the usual Gaussian likelihood of the data conditional on spin parameters $\chi_{1,2}$, $z_{1,2}$ and other parameters (mass, redshift, etc.), which we denote by η . The

next term $\pi(\chi_{1,2}|\alpha_\chi, \beta_\chi, \lambda_0)$ is the EXTENDED model for spin magnitude described in Equation (6). This is followed by $\pi(z_{1,2}|\zeta, \sigma_t, z_{\text{min}})$, which is the EXTENDED model for spin tilts; see Equation (7). The final term $\pi(\eta|\Lambda)$ describes the population model for mass and redshift as well as the usual priors for extrinsic parameters. Our mass model is the POWER LAW + PEAK model from Abbott et al. (2021b) adopted from Talbot & Thrane (2018). Our redshift model is the POWER-LAW EVOLUTION model from Abbott et al. (2021b) adopted from Fishbach et al. (2018).

The likelihood can be written in terms of a non-zero-spin likelihood and a zero-spin likelihood:

$$\mathcal{L}(d|\Lambda) = (1 - \lambda_0) \mathcal{L}_{\chi>0}(d|\Lambda) + \lambda_0 \mathcal{L}_{\chi=0}(d|\Lambda) \quad (\text{A2})$$

where

$$\mathcal{L}_{\chi>0}(d|\Lambda) = \int d\chi_{1,2} \int dz_{1,2} \int d\eta \mathcal{L}(d|\chi_{1,2}, z_{1,2}, \eta) \times \pi(\chi_{1,2}|\alpha_\chi, \beta_\chi) \pi(z_{1,2}|\zeta, \sigma_t, z_{\text{min}}) \pi(\eta|\Lambda) \quad (\text{A3})$$

$$\mathcal{L}_{\chi=0}(d|\Lambda) = \int d\chi_{1,2} \int dz_{1,2} \int d\eta \mathcal{L}(d|\chi_{1,2}, z_{1,2}, \eta) \times \delta(\chi_{1,2}) \pi(z_{1,2}|\zeta, \sigma_t, z_{\text{min}}) \pi(\eta|\Lambda) \quad (\text{A4})$$

$$= \int d\eta \mathcal{L}(d|\chi_{1,2} = 0, z_{1,2}, \eta) \pi(\eta|\Lambda), \quad (\text{A5})$$

using the standard trick for “recycling” posterior samples; see, e.g., Thrane & Talbot (2019). In order to recycle, we rewrite the likelihood in terms of the posterior p , the fiducial evidence $\pi(\theta|\emptyset)$, and the fiducial evidence \mathcal{Z}_\emptyset so that

$$\mathcal{L}_{\chi>0}(d|\Lambda) = \frac{p_{\chi>0}(\Lambda|d)}{\pi(\theta|\emptyset)} \mathcal{Z}_\emptyset. \quad (\text{A6})$$

Then we use the fact that

$$\int d\theta p(\theta) f(\theta) = \frac{1}{n_s} \sum_k f(\theta_k), \quad (\text{A7})$$

to rewrite the integral as a sum over posterior samples. We rewrite $\mathcal{L}_{\chi>0}(d|\Lambda)$ as a sum over n_s fiducial ($\chi > 0$) posterior samples:

$$\mathcal{L}_{\chi>0}(d|\Lambda) = \frac{1}{n_s} \sum_k \left(\frac{\text{Beta}(\chi_{1,2}^k|\alpha_\chi, \beta_\chi)}{\pi(\chi_{1,2}^k|\emptyset)} \right) \times \left(\frac{\pi(z_{1,2}^k|\zeta, \sigma_t, z_{\text{min}})}{\pi(z_{1,2}^k|\emptyset)} \right) \left(\frac{\pi(\eta^k, \dots|\Lambda)}{\pi(\eta^k, \dots|\emptyset)} \right) \mathcal{Z}_\emptyset. \quad (\text{A8})$$

Here, \mathcal{Z}_\emptyset is the fiducial evidence obtained using the fiducial ($\chi > 0$) prior. Likewise, the zero-spin likelihood can be written in terms of the n_0 zero-spin samples:

$$\mathcal{L}_{\chi=0}(d|\Lambda) = \sum_j \left(\frac{\pi(\eta^j, \dots|\Lambda)}{\pi(\eta^j, \dots|\emptyset)} \right) \mathcal{Z}_\emptyset. \quad (\text{A9})$$

Here, \mathcal{Z}_0 is the zero-spin evidence obtained using the zero-spin ($\chi = 0$) prior. Putting everything together, we obtain

$$\begin{aligned} \mathcal{L}(d|\Lambda) &= \frac{1 - \lambda_0}{n_s} \sum_k \left(\frac{\text{Beta}(\chi_{1,2}^k | \alpha_\chi, \beta_\chi)}{\pi(\chi_{1,2}^k | \emptyset)} \right) \\ &\times \left(\frac{\pi(z_{1,2}^k | \zeta, \sigma_t, z_{\min})}{\pi(z_{1,2}^k | \emptyset)} \right) \left(\frac{\pi(\eta^k, \dots | \Lambda)}{\pi(\eta^k, \dots | \emptyset)} \right) \mathcal{Z}_\emptyset \\ &+ \frac{\lambda_0}{n_0} \sum_j \left(\frac{\pi(\eta^j, \dots | \Lambda)}{\pi(\eta^j, \dots | \emptyset)} \right) \mathcal{Z}_0 \\ &= (1 - \lambda_0) \overline{w}_\emptyset(\Lambda) \mathcal{Z}_\emptyset + \lambda_0 \overline{w}_0(\Lambda) \mathcal{Z}_0 \\ &= (1 - \lambda_0) \mathcal{Z}'_\emptyset(\Lambda) + \lambda_0 \mathcal{Z}'_0(\Lambda). \end{aligned} \quad (\text{A10})$$

Here, $\overline{w}_\emptyset(\Lambda)$, $\overline{w}_0(\Lambda)$ are the average importance-sampling weights for the spinning and nonspinning models, respectively. Meanwhile, $\mathcal{Z}'_\emptyset(\Lambda)$, $\mathcal{Z}'_0(\Lambda)$ are the population-weighted Bayesian evidence values for the two subpopulations.

ORCID iDs

Shanika Galaudage  <https://orcid.org/0000-0002-1819-0215>
 Colm Talbot  <https://orcid.org/0000-0003-2053-5582>
 Tushar Nagar  <https://orcid.org/0000-0002-2747-0497>
 Eric Thrane  <https://orcid.org/0000-0002-4418-3895>
 Ilya Mandel  <https://orcid.org/0000-0002-6134-8946>

References

- Abbott, B. P., Abbott, R., Abbott, T. D., et al. 2016, *PhRvL*, **116**, 241103
 Abbott, B. P., Abbott, R., Abbott, T. D., et al. 2019, *ApJL*, **882**, L24
 Abbott, R., Abbott, T. D., Abraham, S., et al. 2020a, *ApJL*, **896**, L44
 Abbott, R., Abbott, T. D., Abraham, S., et al. 2020b, *PhRvL*, **125**, 101102
 Abbott, R., Abbott, T. D., Abraham, S., et al. 2020c, *PhRvD*, **102**, 043015
 Abbott, R., Abbott, T. D., Abraham, S., et al. 2021a, *PhRvX*, **11**, 021053
 Abbott, R., Abbott, T. D., Abraham, S., et al. 2021b, *ApJL*, **913**, L7
 Ashton, G., Hübner, M., Lasky, P. D., et al. 2019, *ApJS*, **241**, 27
 Bavera, S. S., Fragos, T., Qin, Y., et al. 2020, *A&A*, **635**, A97
 Bavera, S. S., Fragos, T., Zevin, M., et al. 2021, *A&A*, **647**, A153
 Belczynski, K., Klencki, J., Fields, C. E., et al. 2020, *A&A*, **636**, A104
 Callister, T. A., Haster, C.-J., Ng, K. K. Y., Vitale, S., & Farr, W. M. 2021, arXiv:2106.00521
 Chia, H. S., Olsen, S., Roulet, J., et al. 2021, arXiv:2105.06486
 Doctor, Z., Wysocki, D., O’Shaughnessy, R., Holz, D. E., & Farr, B. 2019, *ApJ*, **893**, 35
 Farr, B., Holz, D. E., & Farr, W. M. 2018, *ApJL*, **854**, L9
 Farr, W. M., Stevenson, S., Miller, M. C., et al. 2017, *Natur*, **548**, 426
 Fishbach, M., Holz, D. E., & Farr, W. M. 2018, *ApJL*, **863**, L41
 Fuller, J., & Ma, L. 2019, *ApJL*, **881**, L1
 García-Bellido, J., Nuño Siles, J. F., & Ruiz Morales, E. 2021, *PDU*, **31**, 100791
 Gerosa, D., Berti, E., O’Shaughnessy, R., et al. 2018, *PhRvD*, **98**, 084036
 Hannam, M., Schmidt, P., Bohé, A., et al. 2014, *PhRvL*, **113**, 151101
 Husa, S., Khan, S., Hannam, M., et al. 2016, *PhRvD*, **93**, 044006
 Kalogera, V. 2000, *ApJ*, **541**, 319
 Khan, S., Husa, S., Hannam, M., et al. 2016, *PhRvD*, **93**, 044007
 Kimball, C., Talbot, C., Berry, C. P., et al. 2021, *ApJL*, **915**, L35
 Kimball, C., Talbot, C., Berry, C. P. L., et al. 2020, *ApJ*, **900**, 177
 Kumamoto, J., Fujii, M. S., Trani, A. A., & Tanikawa, A. 2021, arXiv:2102.09323
 Kushnir, D., Zaldarriaga, M., Kollmeier, J. A., & Waldman, R. 2016, *MNRAS*, **462**, 844
 Mandel, I., & Broekgaarden, F. S. 2021, arXiv:2107.14239
 Mandel, I., & de Mink, S. E. 2016, *MNRAS*, **458**, 2634
 Mandel, I., & Farmer, A. 2018, arXiv:1806.05820
 Mandel, I., & Fragos, T. 2020, *ApJL*, **895**, L28
 Mandel, I., & O’Shaughnessy, R. 2010, *CQGra*, **27**, 114007
 Mapelli, M. 2020, *FrASS*, **7**, 38
 Mapelli, M. 2021, in *Handbook of Gravitational Wave Astronomy*, ed. C. Bambi, S. Katsanevas, & K. D. Kokkotas (Singapore: Springer), 4
 Marchant, P., Langer, N., Podsiadlowski, P., Tauris, T. M., & Moriya, T. J. 2016, *A&A*, **588**, A50
 Mateu-Lucena, M., Husa, S., Colleoni, M., et al. 2021, arXiv:2105.05960
 Miller, S., Callister, T. A., & Farr, W. M. 2020, *ApJ*, **895**, 128
 Neijssel, C. J., Vinciguerra, S., Vigna-Gómez, A., et al. 2021, *ApJ*, **908**, 118
 Ng, K. K. Y., Vitale, S., Zimmerman, A., et al. 2018, *PhRvD*, **98**, 083007
 Olejak, A., & Belczynski, K. 2021, arXiv:2109.06872
 O’Shaughnessy, R., Gerosa, D., & Wysocki, D. 2017, *PhRvL*, **119**, 011101
 Qin, Y., Fragos, T., Meynet, G., et al. 2018, *A&A*, **616**, A28
 Qin, Y., Marchant, P., Fragos, T., Meynet, G., & Kalogera, V. 2019, *ApJL*, **870**, L18
 Qin, Y., Yuan-Zhu, W., & Dong-Hong, W. 2021, arXiv:2108.04821
 Riley, J., Mandel, I., Marchant, P., et al. 2021, *MNRAS*, **505**, 663
 Rodriguez, C. L., Amaro-Seoane, P., Chatterjee, S., & Rasio, F. A. 2018, *PhRvL*, **120**, 151101
 Rodriguez, C. L., Zevin, M., Pankow, C., Kalogera, V., & Rasio, F. A. 2016, *ApJL*, **832**, L2
 Romero-Shaw, I. M., Talbot, C., Biscoveanu, S., et al. 2020, *MNRAS*, **499**, 3295
 Roulet, J., Chia, H. S., Olsen, S., et al. 2021, *PhRvD*, **104**, 083010
 Roulet, J., & Zaldarriaga, M. 2019, *MNRAS*, **484**, 4216
 Safarzadeh, M., Farr, W. M., & Ramirez-Ruiz, E. 2020, *ApJ*, **894**, 129
 Speagle, J. S. 2020, *MNRAS*, **493**, 3132
 Stevenson, S., Berry, C. P. L., & Mandel, I. 2017, *MNRAS*, **471**, 2801
 Tagawa, H., Haiman, Z., Bartos, I., & Kocsis, B. 2020, *ApJ*, **899**, 26
 Tagawa, H., Haiman, Z., Bartos, I., Kocsis, B., & Omukai, K. 2021, *MNRAS*, **507**, 3362
 Talbot, C., Smith, R. J. E., Thrane, E., & Poole, G. B. 2019, *PhRvD*, **100**, 043030
 Talbot, C., & Thrane, E. 2017, *PhRvD*, **96**, 023012
 Talbot, C., & Thrane, E. 2018, *ApJ*, **856**, 173
 Thrane, E., & Talbot, C. 2019, *PASA*, **36**, E010
 The LIGO Scientific Collaboration, The Virgo Collaboration, Abbott, R., et al. 2021c, arXiv:2108.01045
 Valsecchi, F., Glebbeek, E., Farr, W. M., et al. 2010, *Natur*, **468**, 77
 Wysocki, D., Lange, J., & O’Shaughnessy, R. 2019, *PhRvD*, **100**, 043012
 Zaldarriaga, M., Kushnir, D., & Kollmeier, J. A. 2018, *MNRAS*, **473**, 4174
 Zevin, M., Berry, C. P. L., Coughlin, S., & Chatziioannou, K. 2020, *ApJL*, **899**, L17
 Zevin, M., Pankow, C., Rodriguez, C. L., et al. 2017, *ApJ*, **846**, 82



Erratum: “Building Better Spin Models for Merging Binary Black Holes: Evidence for Nonspinning and Rapidly Spinning Nearly Aligned Subpopulations” (2021, ApJL, 921, L15)

Shanika Galaudage^{1,2}, Colm Talbot³, Tushar Nagar^{1,2}, Deepnika Jain⁴, Eric Thrane^{1,2}, and Ilya Mandel^{1,2,5}

¹School of Physics and Astronomy, Monash University, Clayton VIC 3800, Australia; shanika.galaudage@monash.edu

²OzGrav: The ARC Centre of Excellence for Gravitational Wave Discovery, Clayton VIC 3800, Australia

³LIGO Laboratory, California Institute of Technology, Pasadena, CA 91125, USA

⁴National Institute of Technology Karnataka, Surathkal, Srinivasnagar, 57025, India

⁵Institute of Gravitational Wave Astronomy and School of Physics and Astronomy, University of Birmingham, Birmingham, B15 2TT, UK

Received 2022 July 31; published 2022 September 2

The results in the published version have changed following corrections to our analysis. A bug in our implementation resulted in the prior for the nonspinning submodel being four times larger than it should have been for each event, which incorrectly favored the nonspinning interpretation. Fixing this bug shifts the fraction of binary black holes that are not spinning to lower values ($\lambda_0 = 0.54_{-0.25}^{+0.21}$ at 90% credibility) and reduces the minimum cosine of the spin tilt angle for the spinning black holes ($z_{\min} = -0.27_{-0.45}^{+0.49}$ at 90% credibility). The preference for the EXTENDED model over the DEFAULT model is reduced but is still significant ($\log_{10}(\mathcal{B}) \sim 3.55$ or $\mathcal{B} \sim 3500$; see Table 2). The main conclusions of the publication remain unchanged.

The bug fix results in changes to our hyperparameter posteriors and as a result our population distributions for $\chi_{1,2}$, $\cos(\theta)_{1,2}$, and χ_{eff} have also changed. We present the updated figures and tables following the fixes to our analysis.

The updated population predictive distributions for spin magnitude and spin orientation are shown in Figure 2. The updated posterior distributions for z_{\min} and λ_0 are given in Figure 3. In Figure 4 we present an updated corner plot comparison of the DEFAULT and EXTENDED model hyperparameters. The distribution for χ_{eff} from our updated analysis is given in Figure 5. We see that the spinning and nonspinning subpopulations are not distinct. Further investigation into the fraction of the population with in-plane spins is called for.

We thank Hui Tong for finding this issue.

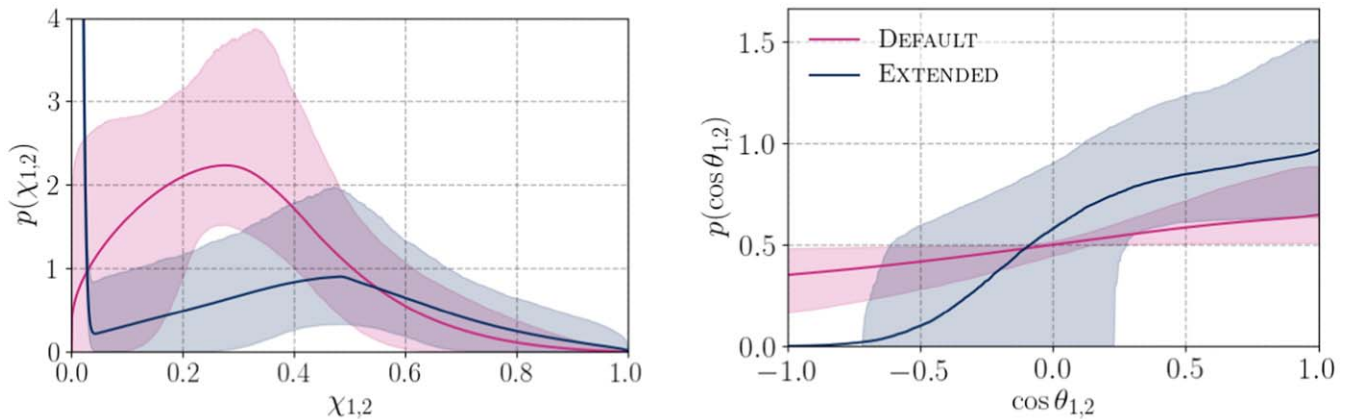


Figure 2. Population predictive distributions for the DEFAULT (pink) and the EXTENDED (navy) models. Left: the distribution of dimensionless spin. Right: the distribution of the cosine of the tilt angle. The solid curves represent the mean and the shaded regions represent the 90% credible interval. In the left-hand panel, we represent the EXTENDED model’s delta function at $\chi = 0$ with a narrow Gaussian with a width of $\sigma_0 = 0.01$ for visibility.

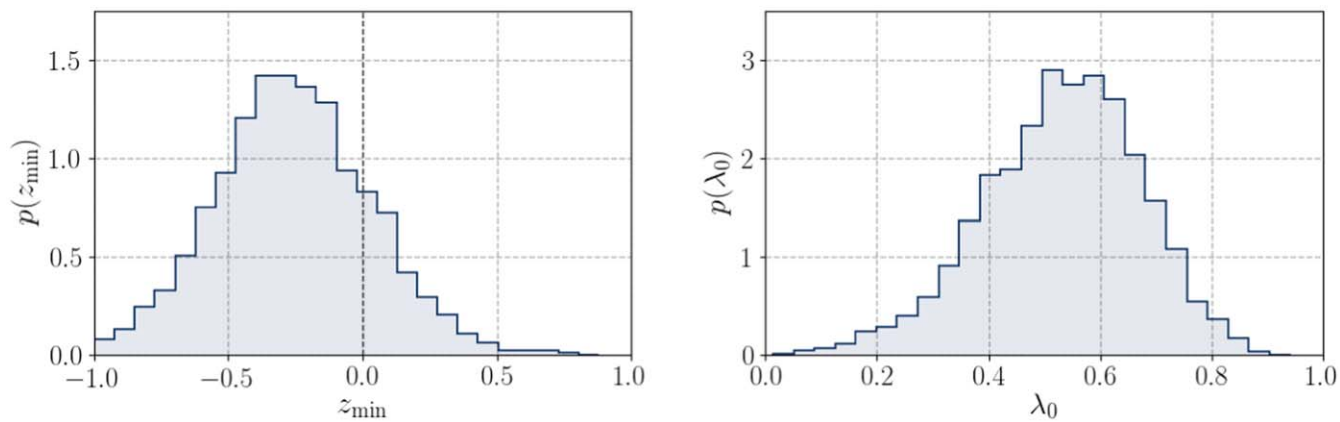


Figure 3. Posterior distributions for population parameters new to the EXTENDED model. Left: the posterior distributions for the population parameter z_{\min} , which determines the minimum cosine tilt angle such that $\cos \theta_{1,2} \geq z_{\min}$. Right: the posterior distribution for λ_0 , the fraction of binaries with negligible black hole spins $\chi_{1,2} = 0$.

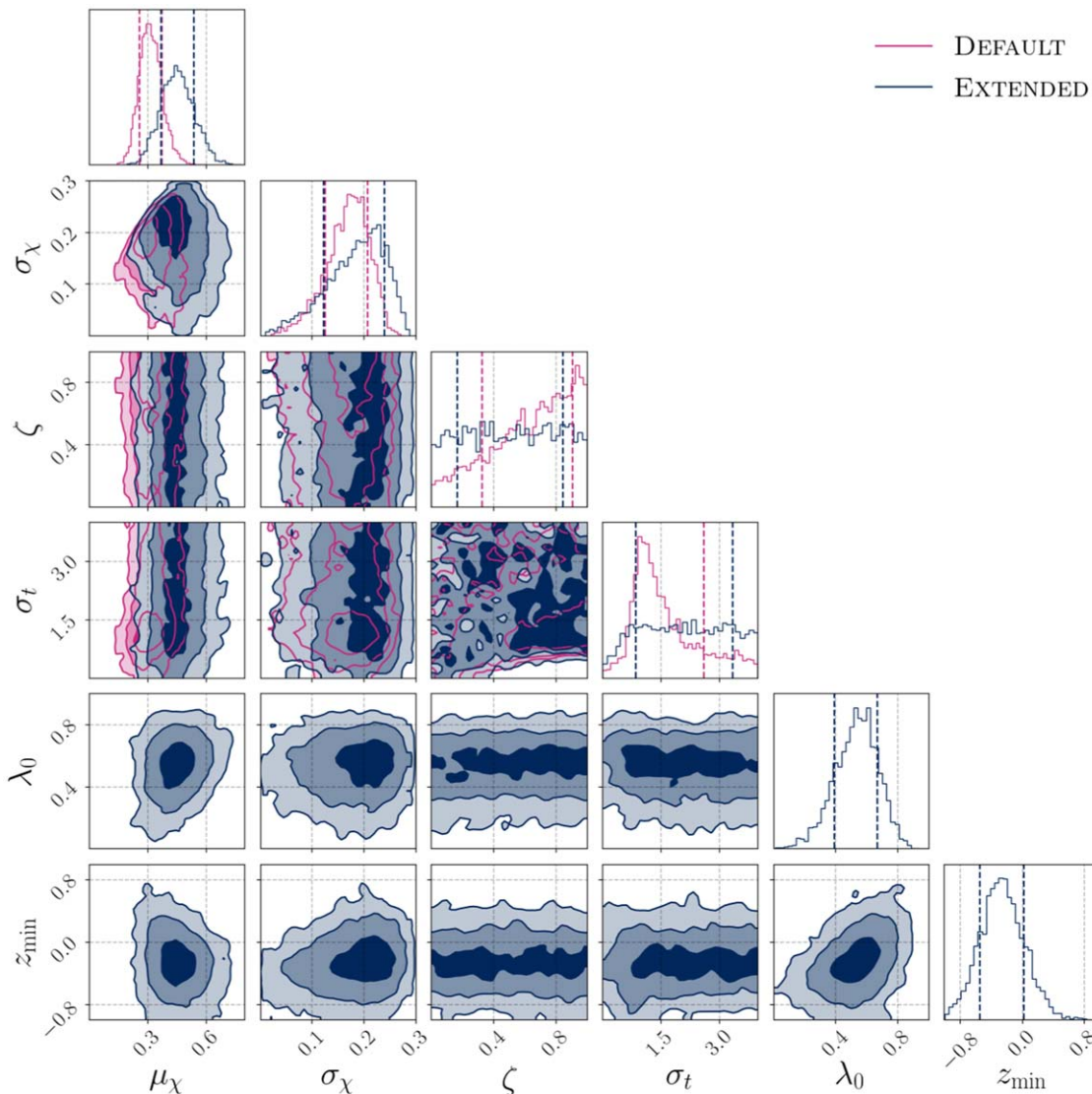


Figure 4. A corner plot showing hyperposterior distributions for the DEFAULT (pink) and EXTENDED (navy) models. The parameters are summarized in Table 2 of the published article. The shaded regions represent 1σ , 2σ , and 3σ credible intervals.

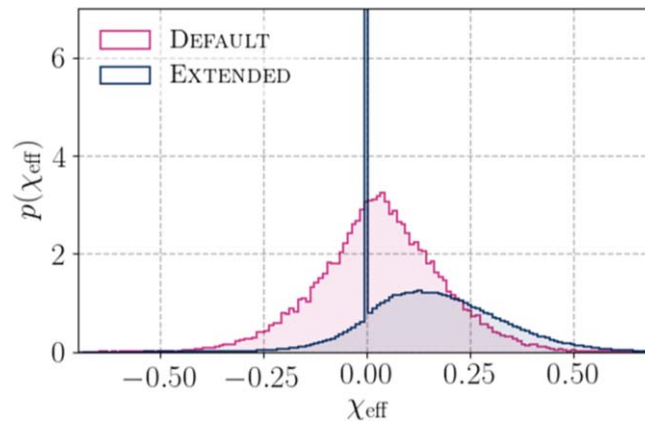







Figure 5. The population predictive distribution for the effective inspiral spin parameter χ_{eff} for the DEFAULT (pink) and the EXTENDED (navy) models.

Table 2
Log Bayes Factors and Maximum Log Likelihood Differences for Different Spin Models Compared to the DEFAULT Model

Spin Model	$\log_{10} \mathcal{B}$	$\Delta \log_{10} \mathcal{L}_{\text{max}}$
DEFAULT	0.00	0.00
EXTENDED	3.55	3.68
EXTENDED with $z_{\text{min}} = 0$	3.94	3.33
EXTENDED with $z_{\text{min}} = -1$	2.87	3.03
EXTENDED with $\lambda_0 = 0$	1.09	0.80

ORCID iDs

Shanika Galaudage  <https://orcid.org/0000-0002-1819-0215>
Colm Talbot  <https://orcid.org/0000-0003-2053-5582>

Tushar Nagar  <https://orcid.org/0000-0002-2747-0497>
Eric Thrane  <https://orcid.org/0000-0002-4418-3895>
Ilya Mandel  <https://orcid.org/0000-0002-6134-8946>